Available online at www.sciencedirect.com

ScienceDirect

Advances in Space Research 66 (2020) 107–115

ADVANCES IN SPACE RESEARCH (a COSPAR publication)

www.elsevier.com/locate/asr

The petitSat mission – Science goals and instrumentation

J. Klenzing [a,*], R.L. Davidson [b], S.L. Jones [a], C. Martinis [c], K.A. Zawdie [d], G.D. Earle [e], J.M. Smith [a,f], A.J. Halford [a], S. Noel [e], N. Paschalidis [g], R.F. Pfaff [a], E. Robertson [e]

[a] NASA Goddard Space Flight Center, ITM Physics Laboratory, Greenbelt, MD 20771, USA
[b] Utah State University, Logan, UT 84322, USA
[c] Boston University, Boston, MA 02215, USA
[d] Naval Research Laboratory, Washington, DC 20375, USA
[e] Space@VT, Virginia Tech, Blacksburg, VA 24061, USA
[f] The Catholic University of America, Washington, DC, 20064, USA
[g] NASA Goddard Space Flight Center, Heliophysics Science Division, Greenbelt, MD 20771, USA

Received 3 September 2019; received in revised form 8 December 2019; accepted 16 December 2019
Available online 24 December 2019

Abstract

The mid- and low-latitude ionosphere is home to a variety of plasma density irregularities, including depletions (bubbles), enhancements (blobs), and small-scale scintillation. Previous studies of plasma density enhancements observed using ROCSAT data have posited that these structures are the direct result of the formation of bubbles near the geomagnetic equator. However, more recent observations from the C/NOFS satellite suggest that multiple mechanisms are responsible for forming plasma enhancements, with wave action in the ionosphere and thermosphere as a significant driver of the enhanced densities. Indeed, statistical analysis of enhancements observed from satellites resembles the statistics of Medium-Scale Traveling Ionosphere Disturbances (MSTIDs) with respect to seasonal variability and solar activity.

petitSat is a CubeSat mission designed to examine the link between MSTIDs and plasma enhancements. The mission will provide in situ measurements of the plasma density, 3D ion drift, as well as ion and neutral composition. The instrument suite includes a combined retarding potential analyzer and cross-track drift meter and an ion-neutral mass spectrometer. This instrument suite will provide comprehensive information about the fluctuations in plasma, as well as changes in the neutral profile. petitSat will launch into a 51 deg inclination orbit at 400 km (consistent with an International Space Station deployment), allowing for numerous conjunctions with the Boston University All-Sky Imager network over the mission lifetime.
Published by Elsevier Ltd on behalf of COSPAR.

Keywords: Cubesat; Ionosphere; MSTID; Plasma irregularities

2010 MSC: 00-01; 99-00

1. Introduction

Understanding the causes of variations in the Earth's ionosphere is one of the key questions in space sciences. A variety of plasma density irregularities have been documented throughout the mid- and low-latitude ionosphere – including depletions (bubbles), enhancements (blobs), and small-scale scintillation. Plasma density depletions – sometimes referred to as plasma bubbles, Spread-F, or convective ionospheric storms – are particularly associated with communications disruptions (*e.g.*, Kelley et al., 2011).

Enhancements in plasma density – sometimes referred to in the literature as blobs – have been frequently observed in

* Corresponding author.
E-mail address: jeffrey.klenzing@nasa.gov (J. Klenzing).

https://doi.org/10.1016/j.asr.2019.12.013
0273-1177/Published by Elsevier Ltd on behalf of COSPAR.

space. There has been considerable debate over the cause of these enhancements, with two major mechanisms highly cited: (a) the nearby formation of plasma bubbles (*e.g.*, Le et al., 2003; Huang et al., 2014), (b) wave action such as MSTIDs (*e.g.*, Choi et al., 2012; Klenzing et al., 2011). It should be noted that there are direct observations of both mechanisms (a) (*e.g.*, Yokoyama et al., 2007) and (b) (*e.g.*, Miller et al., 2014), and therefore it is likely that multiple mechanisms are responsible for these enhancements. However, most statistical studies only focus on the density enhancements and do not distinguish between the relative contributions of these two sources.

The petitSat mission is a 6U CubeSat designed to examine the link between MSTIDs and regions of locally enhanced plasma density, frequently referred to as "plasma blobs." This paper describes the motivation, science goals, and instrumentation of the petitSat mission.

2. Background

2.1. Plasma density enhancements in the ionosphere

Plasma enhancements were first reported from ion density and temperature data from the Hinotori satellite (Oya et al., 1986). They were found beyond the edge of the region of occurrence for bubbles, typically about 15° away from the magnetic equator in either hemisphere, and consisted of an increase in density of a factor of two. Watanabe and Oya (1986) examined the statistics of occurrence and found that enhancements favor the winter hemisphere, typically occur after midnight, and have a strong longitudinal variation that is dependent on season. Based on a statistical analysis of enhancements and depletions encountered by Hinotori, they concluded that the two phenomena must have different physical drivers, with the depletions caused by $\mathbf{E}\times\mathbf{B}$ uplift and the enhancements caused by meridional wind instabilities.

In the following decades, several studies have suggested a stronger link between the evolution of bubbles and blobs. Observations from satellites (Le et al., 2003; Park et al., 2003; Park et al., 2008a, 2008b), all-sky imagers (Pimenta et al., 2004, 2007; Martinis et al., 2009), radar (Yokoyama et al., 2007), and GPS total electron current measurements (Dashora and Pandey, 2005) have shown density enhancements forming simultaneously near depletions. Yokoyama et al. (2007) show depletions and enhancements forming along the same flux tube using data from ROCSAT-1 and Equatorial Atmosphere Radar. Density enhancements were also found along the same field lines as ESF airglow depletions (Martinis et al., 2009) and in between neighboring depleted flux tubes (Pimenta et al., 2007). Statistical studies with satellite data from KOMPSAT-1 and DMSP F15 have shown that the depletions and enhancements show similar seasonal and longitudinal variations (with several exceptions) (Park et al., 2008).

A number of recent studies have shown that other sources can form plasma enhancements and may even be the predominant driver. Kil et al. (2011) showed the formation and evolution of plasma density enhancements with an apparent absence of nearby depletions. Klenzing et al. (2011) analyzed the drift structure within and around the enhancements observed by C/NOFS and found that the drift perturbations perpendicular and parallel to the geomagnetic field could be separated by several hundred km longitudinally (including the events without depletions studied by Kil et al. (2011)). Fig. 1 shows an example of this offset. The top panel shows a typical density enhancement as observed by C/NOFS. The lower panel shows the ion drifts measured both parallel ($v_{\parallel}$) to **B** and in the meridional direction ($v_{\perp m}$, the 'upward' direction in the plane of the magnetic meridian which is perpendicular to **B**). This offset was found to be a persistent feature in the C/NOFS observations (Klenzing et al., 2011), but it was not observed in previous observations from ROCSAT-1 (Le et al., 2003). The differences in orbital inclination alone between the two missions (C/NOFS at 13°, ROCSAT-1 at 35°) are unlikely to explain the phenomena, as the features have been observed consistently for a variety of satellite motions relative to the geomagnetic field lines. Because of this, it is likely that the difference between the C/NOFS and ROCSAT-1 observations is due to different mechanisms acting to create these density enhancements.

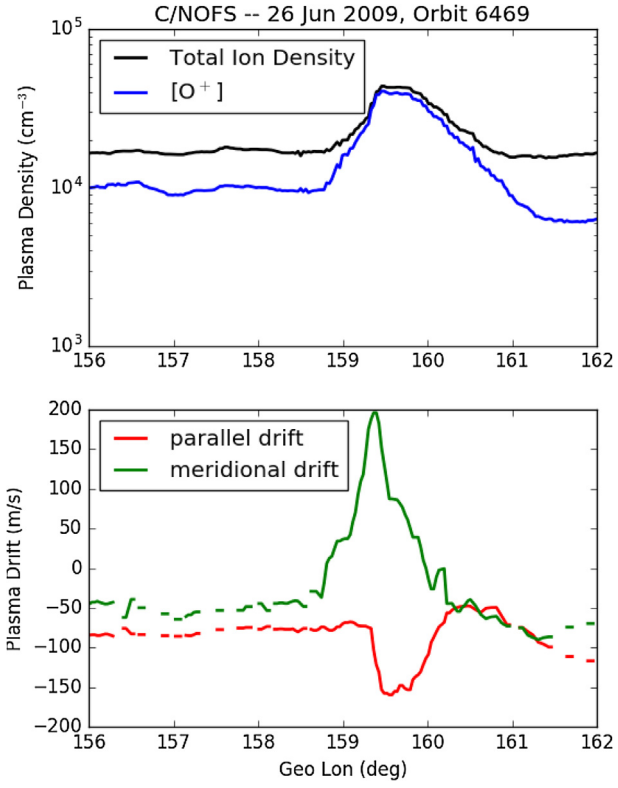

Fig. 1. Plasma density enhancements observed by C/NOFS.

Recent statistical studies from C/NOFS have highlighted the difference in the distributions of enhancements and depletions (*e.g.*, Choi et al., 2012; Haaser et al., 2012). Choi et al. (2012) shows that the enhancements tend to occur at magnetic latitudes greater than ±20° while the depletions tend to occur near the magnetic equator. Additionally, when examined by the apex height distribution, the depletions and enhancements tend to occur on different flux tubes, with the depletions observed by C/NOFS occuring near the satellite perigee (400 km, apex altitude near 500 km for the statistical study) and exponentially decaying with apex altitude, and the observed enhancements peaking near apex altitudes of 1700 km. A key mystery is why these plasma enhancements form on flux tubes farther from the magnetic equator. Possibilities include relative diffusion rates and increased forcing from electric field perturbations. The latter is a likely suspect from comparisons with Medium-Scale Traveling Ionospheric Disturbances (MSTIDs), as discussed in the next section.

2.2. Medium-Scale Traveling Ionospheric Disturbances (MSTIDs)

MSTIDs are quasi-periodic perturbations of the F-layer at midlatitudes with a horizontal scale size of ~100–500 km. The term "MSTID" was coined in the 1960s when ionosonde observations showed periodic upward and downward motion of the ionospheric layer with scale sizes of 100–500 km (medium-scale). An example of these waves seen in all-sky imager data is shown in Fig. 2. They were interpreted as a passive response of the ionosphere to the arrival of neutral atmosphere gravity waves. These waves are a result of gravity restoring equilibrium to perturbations in the neutral atmosphere (Hines, 1960). TIDs driven by gravity waves have been observed over strong Tropospheric storms (*e.g.* (Vadas and Crowley, 2010; Azeem et al., 2015)).

However, other studies have shown that there are strong electric fields associated with TIDs, indicating that the physical mechanisms may be more than a simple passive response to the neutral atmosphere. This was first observed in a study by Behnke (1979) using data from the Arecibo incoherent scatter radar. The first optical observations were carried out at Arecibo by Mendillo et al. (1997) who showed, using all-sky imager observations in 630.0 nm, dark/bright bands of airglow moving equatorward at a significant angle with respect to the magnetic meridian. Additionally, plasma instabilities were embedded inside the bands (Miller et al., 1997; Shiokawa et al., 2003). Conjugate observations of MSTIDs using all-sky imagers in the Japanese sector (Otsuka et al., 2004) suggest that electric fields map from one hemisphere to the other in order to explain the simultaneous observations. Kelley and Makela (2001) postulated that the existence of a polarization electric field would produce the observed southwestward motion. Recently, studies of coupling between sporadic E layer and F region instabilities suggest new insights on the physical mechanisms driving these midlatitude instabilities (Cosgrove and Tsunoda, 2004; Cosgrove, 2007; Yokoyama et al., 2009).

The presence of electric field fluctuations measured at midlatitudes was initially studied by Saito et al. (1995) using DE-2 satellite data. These fluctuations occurred poleward from the crests of the equatorial ionization anomaly and were conjugate in nature. Subsequent studies linked those fluctuations with the presence of MSTIDs and it was recognized that their equatorward and westward motion in both hemispheres was due to polarization electric fields generated in the bands. The scale size of these electric fields is such (~100 km) that they can efficiently map along field lines and, as a consequence, MSTIDs occur simultaneously at conjugate locations and have similar zonal motion. Thus, if one observes an MSTID in one hemisphere, similar structuring will occur in the other hemisphere.

While some observations of electric field fluctuations associated with MSTIDs (Saito et al., 1995; Kelley et al., 2002) did not present perturbations in total ion density, a recent study by Miller et al. (2014) indicated that MSTIDs can be responsible for plasma enhancements observed by satellites at midlatitudes (Kil et al., 2011; Kil et al., 2015). Additionally, MSTIDs have been shown to propagate to the equatorial region, potentially even seeding plasma bubbles there (Takahashi et al., 2018).

2.3. Linking the Phenomena

Previous studies have shown that wave action such as MSTIDs are a likely source of plasma enhancements. Recent observations from Swarm data have shown that these plasma density enhancements can exhibit conjugate behavior similar to that of MSTIDs (Kil et al., 2019). The large electric field perturbations that map to the conjugate hemisphere transport O^+-rich plasma upward, leading

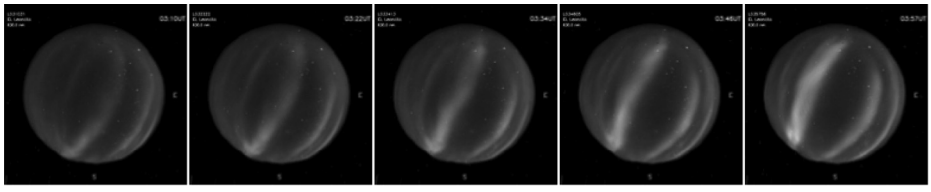

Fig. 2. El Leoncito ASI showing the occurrence of alternating dark and bright 630.0 nm airglow bands, associated with MSTIDs. The motion of the bands is northwestward.

to an enhanced plasma density as observed by a satellite moving through the flux tube connected to the MSTIDs. This is consistent with the observations of plasma enhancements by Klenzing et al. (2011). Indeed, this mechanism also explains the observed offset between the perpendicular and parallel drift.

A westward-propagating source would produce the offset between the parallel and perpendicular plasma flow, as shown in Fig. 3. Here a wave perturbation to the **E**×**B** drift (purple) is moving from east to west just below a given magnetic flux tube (B). For a given region of plasma, the perturbation in the upward (perpendicular) drift peaks at some time interval (t_2), but it still acts to push plasma into the flux tube until it fully passes. The parallel flow is a result of the diffusion forces, and will increase as the density increases. The density (and parallel flow) will peak some time afterward (t_3), resulting in the final configuration in the figure. Note that because this is a continuous process, the configuration at t_1 is always occurring in the flux tube just to the west of t_2. Likewise, the configuration at t_3 also simultaneously occurs just to the east of t_2. Thus a satellite moving from the west to the east will encounter each of these configurations in order, resulting in a spatial separation observed between the max perpendicular and parallel drifts, as observed in Fig. 1.

The C/NOFS satellite provided many important clues about the relation of plasma enhancements to other phenomena, however, the narrow orbital inclination (13°) limited the potential observations of this phenomena that typically occurs at higher latitudes. Despite this narrow inclination, several observations of density enhancements associated with MSTIDs were published (*e.g.*, Miller et al., 2014). Possible conjunctions with ground-based imagers such as Arecibo were limited to higher altitudes well above the F-peak. petitSat will have instrumentation similar to C/NOFS, but will fly in a 51° inclination orbit in order to better examine the variation of this phenomena with magnetic latitude. The increased data sampling at the middle latitudes will allow for increased observations of the ionosphere over MSTIDs.

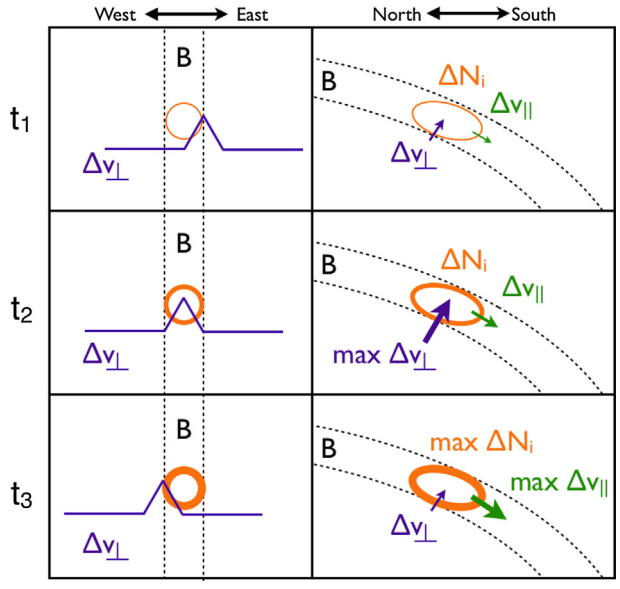

Fig. 3. E-field perturbations due to MSTIDs explain the offset between the parallel and perpendicular flow. Figure after Klenzing et al. (2011).

3. Science goals

The petitSat mission has two primary goals:

(1) Systematically identify and classify ionospheric plasma density enhancements in the nightside mid-and low-latitude region, including changes in ion motion, plasma properties, and the thermospheric background associated with them. The identification of density enhancements is a fairly straightforward procedure. Here we will identify not only the enhanced density, but associated changes in drifts and composition, including the offset between the drift parallel and perpendicular to **B**. Modification of the inputs will be incorporated to run sensitivity studies similar to ? (Klenzing et al., 2013). Statistics will be compiled over six months of data (one solstice and one equinox) over all longitudes.

(2) Combine this space-borne database with ground-based identification of MSTIDs to quantify their relative contribution to the generation of plasma enhancements in the ionosphere. For each conjunction of petitSat with an ASI observation, the existence of plasma enhancements at the satellite and MSTIDs at the geomagnetic footprint will be identified. Over the course of the six-month mission, the relative frequencies of plasma enhancements occurring both with and without associated MSTIDs can be identified and quantified as a function of location, local time, *etc*. Local fluctuations in the neutral density and composition will provide key information about the existence of local neutral waves that could modify the measured plasma.

4. Instrumentation

The petitSat mission will provide in situ measurements of the plasma density, 3D ion drift, as well as ion and neutral composition. This instrument suite will provide comprehensive information about the fluctuations in plasma, as well as changes in the neutral profile. This section describes the instrument suite on the petitSat satellite in detail.

4.1. GRIDS – Gridded Retarding Ion Drift Sensor

The GRIDS instrument provides measurements of the ion density, drift, composition, and temperature. It combines two well-known analysis techniques for thermal plasma to achieve this: 1) retarding potential analysis and 2) cross-track drift analysis. The engineering unit for the petitSat mission is shown in Fig. 4.

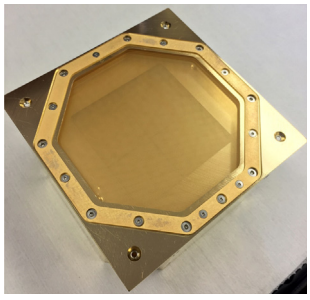

Fig. 4. The GRIDS instrument.

Retarding potential analysis (RPA) has a long history of providing in situ diagnostics of the thermal ion distribution in the Earth's ionosphere. The practical and theoretical background of the technique are well described in the literature (Whipple, 1959; Knudsen, 1966; Chao et al., 2003; Davidson and Earle, 2011), and RPA instruments have successfully flown on many large satellite missions, including Dynamics Explorer (DE) (Hanson et al., 1981), Atmosphere Explorer (AE) (Hanson et al., 1973), and the Detection of Electro-Magnetic Emissions Transmitted from Earthquake Regions (DEMETER) satellite (Berthelier et al., 2006). When coupled with good spacecraft velocity data and attitude knowledge, analysis of the current–voltage characteristics produced by an RPA provides measurements of the overall plasma density, the ion temperature, the component of the ion velocity along the orbit-track, and the relative composition of ions such as H^+ and O^+ in planetary ionospheres.

It has also led to the pairing of an RPA with a complementary instrument designed to measure the remaining two components of the ion drift velocity vector. Often referred to as an Ion Drift Meter (IDM), this instrument has been utilized along with the RPA. While this pairing offers an extremely comprehensive, robust, and relatively small instrument package, it is often still too large to be utilized on a CubeSat. The GRIDS instrument combines the functions of the RPA and IDM into one sensor head and is specifically designed for compatibility with the size, mass, and power restrictions required by CubeSat platforms.

The GRIDS sensor head consists of a square aperture that is mounted on the ram face of a CubeSat. The aperture is made as small as possible (to reduce the impact of non-uniform sheath effects near the edges of the spacecraft) while still maintaining enough signal to remain functional in the ionospheric regions of interest. Behind the aperture is a series of biased and grounded grids that act as ion-energy filters. When the instrument is in RPA mode, one of these grids is swept over a range of voltages and acts in the same manner as the retarding grid would in an RPA. When in IDM mode, one grid is held at a static potentials sufficient to screen out light ions. At the back of the instrument are four segmented collector elements. As ions impact these segments they exchange charge with the conductive surface which is measured as a current by the GRIDS electronics. In RPA mode the current from the four segments is added together to allow for the calculation of the total ion flux as a function of retarding voltage which can then be related to ion density, temperature, relative concentration of heavy to light ions, and the component of the velocity vector normal to the instrument face. In IDM mode, ratios of the currents collected by pairs of collector segments are calculated. When combined with knowledge of the instrument dimensions and grid configuration, these ratios allow for the calculation of the arrival angle of the incoming ion beam through the aperture. The angle and ram velocity component determined when in RPA mode can be combined for the complete determination of the three dimensional ion drift velocity vector.

For the petitSat mission, RPA mode and IDM mode will be interleaved to complete an entire measurement cycle in 2 s. A full list of the expected measurements and instrument operational parameters for GRIDS is shown in Table 1. The GRIDS electronics draw direct lineage from the RPA electronics designed for the LAICE CubeSat mission that is planned to launch in 2020 (Westerhoff et al., 2015).

4.2. INMS

The Ion Neutral Mass Spectrometer (INMS) provides measurements of ion and neutral composition, i.e. relative density of the various species, and total ion and neutral density using the time of flight method.

Time of flight (TOF) mass spectrometry has a long history of providing in situ diagnostics of the thermal ion and neutral distribution in Earth's ionosphere and thermosphere. The practical and theoretical background of the technique are well described in the literature (Hedin et al., 1973; Nier et al., 1973; Peiz et al., 1973; Carignan et al., 1981), and TOF mass spectrometer instruments have successfully flown on large satellite missions, including Dynamics Explorer (DE). When coupled with the use of

Table 1
GRIDS specifications.

Parameter		Specification
Velocity	Range	−1500 m/s to 1500 m/s
	Accuracy	±10 m/s
Ion Density	Range	5×10^3 cm^{-3} to 5×10^7 cm^{-3}
	Accuracy	500 cm^{-3} or 2%
Ion Temperature	Range	0 K to 3000 K
	Accuracy	10 K or 5%
Composition (H^+, He^+, O^+)	Range	0 to 1
	Accuracy	0.02
Dimensions		0.75 U
Mass		0.5 kg
Power		0.5 W
Measurement Cadence		0.5 Hz
Data Rate		533 bit/s
Operating Temperature		−20 °C to 80 °C

pre-acceleration to reduce the energy dispersion of incoming particles, the mass of each particle is calculated from its TOF through a section of the instrument of known length. The petitSat INMS measures species including H, He, N, O, N_2 and O_2 with M/dM of approximately 12. A full list of the expected measurements and instrument operational parameters for INMS is shown in Table 2.

The INMS is based on front end optics with pre-acceleration, gated time-of-flight, an electrostatic analyzer and channel electron multiplier detectors. The neutral front-end optics include thermionic emission ionization and ion blocking grids. The electronics include front-end, fast gating, high voltage power supply, ionizer, time of flight binning and full bi-directional command and data handling digital electronics. The data package includes 400 mass bins each for both ions and neutrals and key housekeeping data for instrument health and calibration. For petitSat, the data rate is one sample per second. This miniaturized instrument fits within a 1.3 U volume (8.3 cm × 9.2 cm × 16 cm), weighs approximately 1 kg and requires nominal power of roughly 1.8 W.

A sample of the neutral mass spectrum as measured in the laboratory environment is shown in Fig. 5 (Rodriguez et al., 2016). This represents the ambient gas in the chamber. The INMS has flight heritage from the Ion Neutral Mass Spectrometer flown on the ExoCube and Dellingr CubeSat missions (Fig. 6), however, these missions were not three-axis stabilized and scientific interpretation of these datasets is ongoing. The instrument was integrated into the ExoCube2 bus, has successfully completed environmental testing and is expected to launch in 2020.

5. All-sky Imagers

In order to complete Science Goal 2, the petitSat mission will work with extensive ground-based observatories as part of campaigns. petitSat will launch into a 51° inclination orbit at 400 km (consistent with an International Space Station deployment), allowing for numerous conjunctions with the Boston University All-Sky Imager network over the mission lifetime.

All-sky imagers (ASIs) are used to measure mesosphere and thermosphere airglow emissions (Martinis et al., 2006).

Table 2
INMS specifications.

Parameter	Performance
Ion Species	H^+, He^+, N^+, O^+, NO^+, O_2^+
Ion Range	10^3 cm^{-3} to 10^7 cm^{-3}
Neutral Species	H, He, N, O, N_2, and O_2
Neutral Range	10^5 cm^{-3} to 10^9 cm^{-3}
Volume	1.3 U
Mass	960 g
Power	1.8 W
Measurement Cadence	1 s
Data Rate	13.1 kbit/s
Operating Temperature	−10 °C to 50 °C

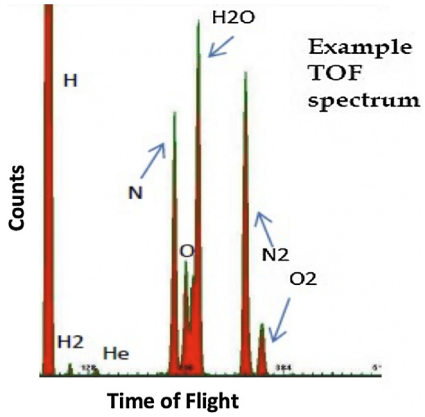

Fig. 5. Laboratory Neutral Mass Spectrum from INMS.

The Boston University all-sky imager network (Martinis et al., 2018) provide measurements of MSTIDs covering a large area and providing 2D information on their characteristics during conjunctions with petitSat. This network consists of 13 imagers distributed worldwide from equatorial to sub-auroral latitudes that allows the study of diverse ionospheric processes. Relevant to this project is the use of information from 8 ASIs located at low and mid latitudes. Fig. 7 shows the locations and fields-of-view of the imagers of interest in the American sector, along with the range of latitudes sampled by petitSat at 400 km altitude. Each circle represents the field of view for an emission height of 300 km and zenith angles down to 80 degrees. Comparisons with additional imagers will be incorporated as available.

Each ASI consists of a fish-eye lens at the top, an optical assembly, a filter wheel that houses six four-inch narrow band (∼10 Å) interference filters, and a back-illuminated thinned CCD. The detector assembly is housed in a thermoelectrically cooled chamber capable of cooling to −60° below the ambient temperature. The field of view of the instrument is 180°. The resulting 25 mm diameter filtered image is formed at F/1.5 on the CCD. Interference filters to isolate particular airglow emission lines are used to study mesospheric and thermospheric processes. The optical arrangement is such that a ray arriving at 90° from zenith reaches the filter at an angle of ∼4°, thus the peak transmission of the filter at the nightglow wavelength is high, >80%, for all the rays coming from the sky. The measurement parameters of the imagers are found in Table 3.

The system takes images at several wavelengths for the duration of the night on nearly every night in a given month. Thermospheric emissions of neutral oxygen are measured at wavelengths of 630.0 nm, 777.4 nm, and 557.7 nm. Mesospheric processes are studied by measuring emissions at 589.3 nm (Na), 557.7 nm and OH lines with $\lambda > 695.0$ nm. A background filter at 644.4 nm is used as a control filter. Light measured with this filter does not come from any particular atmospheric source. Exposure times are 90 or 120 s (depending on the site) for all the filters except OH, which has an exposure time of 30 s. An

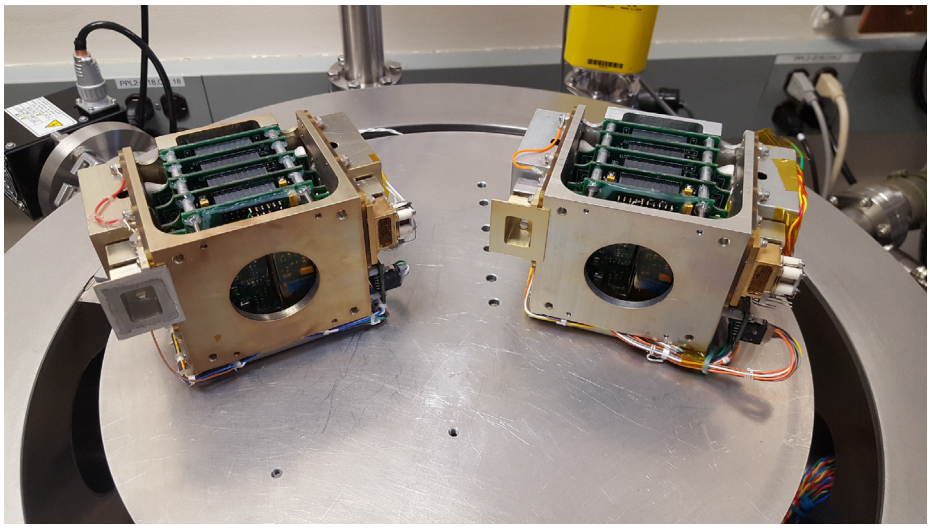

Fig. 6. The INMS Flight and Engineering Units as delivered to Dellingr.

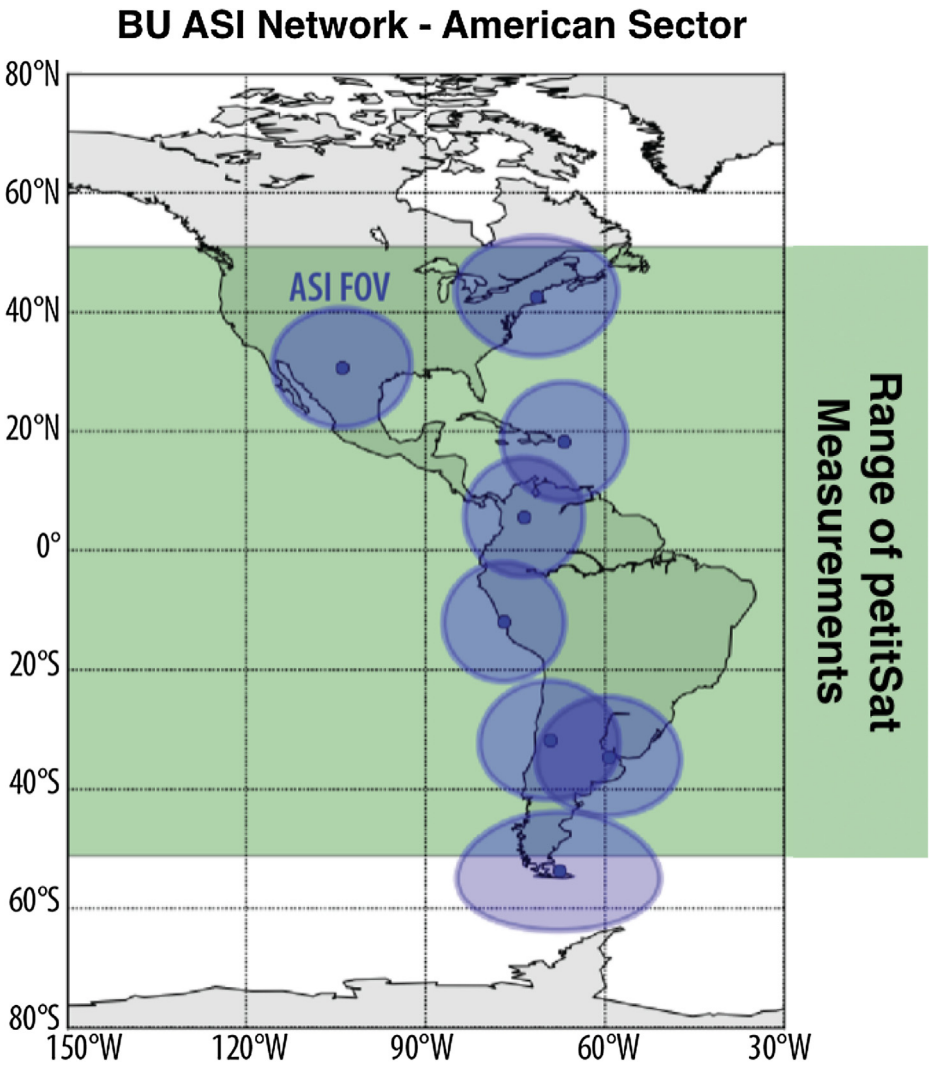

Fig. 7. Potential conjunctions of petitSat with the BU imager network in the American Sector.

Table 3
ASI specifications.

Parameter	Specification
Emission Wavelength	630.0 nm
Exposure Time	90 or 120 s
Horizontal Resolution	30 km × 30 km
Temporal Resolution	10 min

entire cycle of observations takes ~10 min. The only nights when data are not taken are those within a day of full Moon, so data are collected on 27–28 nights per month. Quick-look images and movies can be seen at www.buimaging.com.

The structures we are investigating are MSTIDs, *i.e.*, tilted dark and bright bands detected in 630.0 nm. MSTIDs have large scale electric field perturbations and thus one should be able to detect them, or their effects, anywhere along the field line, as shown by Saito et al. (1995). Additional imagers are located at Asiago and New Zealand. This work uses images taken at 630.0 nm, an airglow emission produced by the de-excitation of the O^1D atomic oxygen state. The images are spaced about 10 min apart. When dealing with MSTIDs, wave patterns showing dark (bright) regions represent upward (downward) motions of the ionospheric layer that can be related to zonal electric field perturbations.

6. Summary

The petitSat mission is a 6U CubeSat designed to examine the link between MSTIDs and regions of locally enhanced plasma density, frequently referred to as "plasma blobs." The instrumentation suite will provide in situ measurements of plasma density, 3D ion drift as well as the ion and neutral composition. The data from the instrument suite will be correlated with ground based measurements from all-sky imagers. The goals of the mission are to determine the drift, density and O^+/H^+ signatures of plasma enhancements as a function of magnetic latitude and to quantify the contribution of MSTIDs to the generation of plasma enhancements in the ionosphere.

Declaration of Competing Interest

The authors declare that they have no known competing financial interests or personal relationships that could have appeared to influence the work reported in this paper.

Acknowledgements

The petitSat Mission is funded through NASA grant NNH16ZDA001N-HTIDS. K. Zawdie acknowledges support from the Chief of Naval Research (CNR) under the NRL 6.1 Base Program.

References

Azeem, I., Yue, J., Hoffmann, L., Miller, S.D., Straka III, W.C., Crowley, G., 2015. Multisensor profiling of a concentric gravity wave event propagating from the troposphere to the ionosphere. Geophys. Res. Lett. 42, 7874–7880. https://doi.org/10.1002/2015GL065903.

Behnke, R.A., 1979. F-layer height bands in the nocturnal ionosphere over Arecibo. J. Geophys. Res. 84 (A3), 974–978. https://doi.org/10.1029/JA084iA03p00974.

Berthelier, J.J., Godefroy, M., Leblanc, F., Seran, E., Peschard, D., Gilbert, P., Artrub, J., 2006. IAP, the thermal plasma analyzer on DEMETER. Planet. Space Sci. 54, 487–501.

Carignan, G.R., Block, B.P., Maurer, J.C., Hedin, A.E., Reber, C.A., Spencer, N.W., 1981. The neutral mass spectrometer on Dynamics Explorer B. Space Sci. Instrum. 5, 429–441.

Chao, C.K., Su, S.-Y., Yeh, H.C., 2003. Grid effects on the derived ion temperature and ram velocity from the simulated results of the retarding potential analyzer data. Adv. Space Res. 32, 2361–2366.

Choi, H.S., Kil, H., Kwak, Y.S., Park, Y.D., Cho, K.S., 2012. Comparison of the bubble and blob distributions during the solar minimum. J. Geophys. Res. 117 (A4), A04314. https://doi.org/10.1029/2011JA017292.

Cosgrove, R.B., 2007. Generation of mesoscale F-layer structure and electric fields by the combined Perkins and Es layer instabilities, in simulations. Ann. Geophys. 25, 1579–1601.

Cosgrove, R.B., Tsunoda, R.T., 2004. Instability of the E-F coupled nighttime midlatitude ionosphere. J. Geophys. Res. 109, A04305. https://doi.org/10.1029/2003JA010243.

Dashora, N., Pandey, R., 2005. Observations in equatorial anomaly region of total electron content enhancements and depletions. Ann. Geophys. 23, 2449–2456.

Davidson, R.L., Earle, G.D., 2011. A design approach for improving the performance of single-grid planar retarding potential analyzers. Phys. Plasmas 18, 012905.

Haaser, R.A., Earle, G.D., Heelis, R.A., Klenzing, J., Stoneback, R., Coley, W.R., Burrell, A.G., 2012. Characteristics of low-latitude ionospheric depletions and enhancements during solar minimum. J. Geophys. Res. 117 (A10), A10305. https://doi.org/10.1029/2012JA017814.

Hanson, W.B., Zuccaro, D.R., Lippincott, C.R., Sanatani, S., 1973. The retarding-potential analyzer on Atmosphere Explorer. Radio Sci. 8, 333–339.

Hanson, W.B., Heelis, R.A., Power, R.A., Lippincott, C.R., Zuccaro, D. R., Holt, B.J., Harmon, L.H., Sanatani, S., 1981. The retarding potential analyzer for dynamics explorer-B. Space Sci. Instrum. 5, 503–510.

Hedin, A.E., Mayr, H.G., Reber, C.A., Carignan, G.R., Spencer, N.W., 1973. A global empirical model of thermospheric composition based on Ogo-6 mass spectrometer measurements. Space Res. 13, 315–320.

Hines, C.O., 1960. Internal atmospheric gravity waves at ionospheric heights. Can. J. Phys. 38, 1441–1481.

Huang, C.-S., Le, G., de La Beaujardiere, O., Roddy, P.A., Hunton, D.E., Pfaff, R.F., Hairston, M.R., 2014. Relationship between plasma bubbles and density enhancements: Observations and interpretation. J. Geophys. Res. Space Phys. 119, 1325–1336. https://doi.org/10.1002/2013JA019579.

Kelley, M., Makela, J., 2001. Resolution of the discrepancy between experiment and theory of midlatitude F-region structures. Geophys. Res. Lett. 28 (11), 2589–2592. https://doi.org/10.1029/2000GL012777.

Kelley, M.C., Makela, J.J., Saito, A., 2002. The mid-latitude F region at the mesoscale: some progress at last. J. Atmos. Solar-Terr. Phys. 64, 1525–1529.

Kelley, M.C., Makela, J.J., de La Beaujardiére, O., Retterer, J., 2011. Convective ionospheric storms: a review. Rev. Geophys. Space Phys. 49, RG2003. https://doi.org/10.1029/2010RG000340.

Kil, H., Choi, H.S., Heelis, R.A., Paxton, L.J., Coley, W.R., Miller, E.S., 2011. Onset conditions of bubbles and blobs: A case study on 2 March

2009. Geophys. Rev. Lett. 38 (6), L06101. https://doi.org/10.1029/2011GL046885.

Kil, H., Kwak, Y.-S., Lee, W.K., Miller, E.S., Oh, S.-J., Choi, H.-S., 2015. The causal relationship between plasma bubbles and blobs in the low-latitude F region during a solar minimum. J. Geophys. Res. Space Phys. 120, 3961–3969. https://doi.org/10.1002/2014JA020847.

Kil, H., Paxton, L.J., Jee, G., Nikoukar, R., 2019. Plasma blobs associated with medium-scale traveling ionospheric disturbances. Geophys. Res. Lett. 46, 3575–3581. https://doi.org/10.1029/2019GL082026.

Klenzing, J., Burrell, A.G., Heelis, R.A., Huba, J.D., Pfaff, R., Simões, F., 2013. Exploring the role of ionospheric drivers during the extreme solar minimum of 2008. Ann. Geophys. 31 (12), 2147–2156. https://doi.org/10.5194/angeo-31-2147-2013.

Klenzing, J.H., Rowland, D.E., Pfaff, R.F., Le, G., Freudenreich, H., Haaser, R.A., Burrell, A.G., Stoneback, R.A., Coley, W.R., Heelis, R. A., 2011. Observations of low-latitude plasma density enhancements and their associated plasma drifts. J. Geophys. Res. 116, A09324. https://doi.org/10.1029/2011JA016711.

Knudsen, W.C., 1966. Evaluation and demonstration of the use of retarding potential analyzers for measuring several ionospheric quantities. J. Geophys. Res. 71, 4669–4678.

Le, G., Huang, C.-S., Pfaff, R.F., Su, S.-Y., Yeh, H.-C., Heelis, R.A., Rich, F.J., Hairston, M., 2003. Plasma density enhancements associated with equatorial spread F: ROCSAT-1 and DMSP observations. J. Geophys. Res. 108 (A8), 1318. https://doi.org/10.1029/2002JA009592.

Martinis, C., Baumgardner, J., Smith, S.M., Colerico, M., Mendillo, M., 2006. Imaging science at El Leoncito. Ann. Geophys. 24, 1375–1385. https://doi.org/10.5194/angeo-24-1375-2006.

Martinis, C., Baumgardner, J., Mendillo, M., Su, S.-Y., Aponte, N., 2009. Brightening of 630.0 nm equatorial spread-F airglow depletions. J. Geophys. Res. 114, A06318. https://doi.org/10.1029/2008JA013931.

Martinis, C., Baumgardner, J., Wroten, J., Mendillo, M., 2018. All-sky-imaging capabilities for ionospheric space weather research using geomagnetic conjugate point observing sites. Adv. Space Res. 61 (7), 1636–1651. https://doi.org/10.1016/j.asr.2017.07.021.

Mendillo, M., Baumgardner, J., Nottingham, D., Aarons, J., Reinisch, B., Scali, J., Kelley, M., 1997. Investigations of thermospheric-ionospheric dynamics with 6300-Å images from the Arecibo Observatory. Pub. Astro. Soc. Pac. 125, 7331–7343. https://doi.org/10.1029/96JA02786.

Miller, C.A., Swartz, W.E., Kelley, M.C., Mendillo, M., Nottingham, D., Scali, J., Reinisch, B., 1997. Electrodynamics of midlatitude spread F: 1. Observations of unstable, gravity wave-induced ionospheric electric fields at tropical latitudes. J. Geophys. Res. 102 (A6), 11521–11532. https://doi.org/10.1029/96JA03839.

Miller, E.S., Kil, H., Makela, J.J., Heelis, R.A., Talaat, E.R., Talaat, E., Gross, A., 2014. Topside signature of medium-scale traveling ionospheric disturbances. Ann. Geophys. 32 (8), 959–965. https://doi.org/10.5194/angeo-32-959-2014.

Nier, A.O., Potter, W.E., Hickman, D.R., Mauersberger, K., 1973. The open-source neutral-mass spectrometer on Atmosphere Explorer C, D, and E. Radio Sci. 8, 271–276.

Otsuka, Y., Shiokawa, K., Ogawa, T., Wilkinson, P., 2004. Geomagnetic conjugate observations of medium-scale traveling ionospheric disturbances at midlatitude using all-sky airglow imagers. Geophys. Res. Lett. 31, L15803. https://doi.org/10.1029/2004GL020262.

Oya, H., Takahashi, T., Watanabe, S., 1986. Observations of low latitude ionosphere by the impedance probe on board the Hinotori satellite. J. Geomagn. Geoelectr. 38, 111–123.

Park, J., Min, K.W., Lee, J.-J., Kil, H., Kim, V.P., Kim, H.-J., Lee, E., Lee, D.Y., 2003. Plasma blob events observed by KOMPSAT-1 and DMSP F15 in the low latitude nighttime upper ionosphere. Geophys. Res. Lett. 30 (21), 2114. https://doi.org/10.1029/2003GL018249.

Park, J., Min, K.W., Kim, V.P., Kil, H., Kim, H.J., Lee, J.J., Lee, E., Kim, S.J., Lee, D.Y., Hairston, M., 2008. Statistical description of low-latitude plasma blobs as observed by DMSP F15 and KOMPSAT-1. Adv. Space Res. 41, 650–654. https://doi.org/10.1016/j.asr.2007.04.089.

Park, J., Stolle, C., Luhr, H., Rother, M., Su, S.-Y., Min, K.W., Lee, J.-J., 2008. Magnetic signatures and conjugate features of low-latitude plasma blobs as observed by the CHAMP satellite. J. Geophys. Res. 113, A09313. https://doi.org/10.1029/2008JA013211.

Peiz, D.T., Reber, C.A., Hedin, A.E., Carignan, G.R., 1973. A neutral-atmosphere composition experiment for the Atmosphere Explorer C, D, and E. Radio Sci. 8, 277–285.

Pimenta, A.A., Sahai, Y., Bittencourt, J.A., Abdu, M.A., Takahashi, H., Taylor, M.J., 2004. Plasma blobs observed by ground-based optical and radio techniques in the Brazilian tropical sector. Geophys. Res. Lett. 31, L12810. https://doi.org/10.1029/2004GL020233.

Pimenta, A.A., Sahai, Y., Bittencourt, J.A., Rich, F.J., 2007. Ionospheric plasma blobs observed by OI 630 nm all-sky imaging in the Brazilian tropical sector during the major geomagnetic storm of April 6–7, 2000. Geophys. Res. Lett. 34, L02820. https://doi.org/10.1029/2006GL028529.

Rodriguez, M., Paschalidis, N., Jones, S., Sittler, E., Chornay, D., Uribe, P., Cameron, T., 2016. Miniaturized Ion and Neutral Mass Spectrometer for CubeSat Atmospheric Measurements. NASA Technical Reports Server, Document 20160010304..

Saito, A., Iyemori, T., Sugiura, M., Maynard, N.C., Aggson, T.L., Brace, L.H., Takeda, M., Yamamoto, M., 1995. Conjugate occurrence of the electric field fluctuations in the nighttime midlatitude ionosphere. J. Geophys. Res. 100 (A11), 21439–21451. https://doi.org/10.1029/95JA01505.

Shiokawa, K., Otsuka, Y., Ihara, C., Ogawa, T., Rich, F.J., 2003. Ground and satellite observations of nighttime medium-scale traveling ionospheric disturbance at midlatitude. J. Geophys. Res. 108 (A4), 1145. https://doi.org/10.1029/2002JA009639.

Takahashi, H., Wrasse, C.M., Figueiredo, C.A.O.B., Barros, D., Abdu, M.A., Otsuka, Y., Shiokawa, K., 2018. Equatorial plasma bubble seeding by MSTIDs in the ionosphere. Prog. Earth Planet. Sci. 5, 32. https://doi.org/10.1186/s40645-018-0189-2.

Vadas, S.L., Crowley, G., 2010. Sources of the traveling ionospheric disturbances observed by the ionospheric TIDDBIT sounder near Wallops Island on 30 October 2007. J. Geophys. Res. 115, A07324. https://doi.org/10.1029/2009JA015053.

Watanabe, S., Oya, H., 1986. Occurrence characteristics of low latitude ionosphere irregularities observed by impedance probe on board the Hinotori satellite. J. Geomagn. Geoelectr. 38, 125–149.

Westerhoff, J., Earle, G., Bishop, R.L., Swenson, G.R., Vadas, S., Clemmons, J., Davidson, R., Fanelli, L., Fish, C., Garg, V., Ghosh, A., Kroeker, E., Marquis, P., Martin, D., Noel, S., Orr, C., Robertson, R., 2015. LAICE CubeSat mission for gravity wave studies. Adv. Space Res. 56, 1413–1427. https://doi.org/10.1016/j.asr.2015.06.036.

Whipple, E.C., 1959. The ion-trap results in exploration of the upper atmosphere with the help of the third Soviet sputnik. Proc. IRE 47, 2023–2024.

Yokoyama, T., Su, S.-Y., Fukao, S., 2007. Plasma blobs and irregularities concurrently observed by ROCSAT-1 and Equatorial Atmosphere Radar. J. Geophys. Res. 112, A05311. https://doi.org/10.1029/2006JA012044.

Yokoyama, T., Hysell, D.L., Otsuka, Y., Yamamoto, M., 2009. Three-dimensional simulation of the coupled Perkins and Es-layer instabilities in the nighttime midlatitude ionosphere. J. Geophys. Res. 114, A03308. https://doi.org/10.1029/2008JA013789.